Applied Numerical Mathematics 153 (2020) 98–113

Contents lists available at ScienceDirect

Applied Numerical Mathematics

www.elsevier.com/locate/apnum

A meshfree finite volume method with optimal numerical integration and direct imposition of essential boundary conditions

Hengguang Li [a,1], Qinghui Zhang [b,*,2]

[a] Department of Mathematics, Wayne State University, Detroit, MI 48202, USA
[b] Guangdong Province Key Laboratory of Computational Science and School of Data and Computer Science, Sun Yat-Sen University, Guangzhou, 510006, PR China

ARTICLE INFO

Article history:
Received 6 July 2019
Accepted 9 February 2020
Available online 13 February 2020

Keywords:
Meshfree method
Finite volume method
Essential boundary condition
Numerical integration

ABSTRACT

Meshfree methods (MMs) enjoy advantages in discretizing problem domains over mesh-based methods. Extensive progress has been made in the development of the MMs in the last three decades. The commonly used MMs, such as the reproducing kernel particle methods (RKP), the moving least-square methods (MLS), and the meshless Petrov-Galerkin methods, have main difficulties in numerical integration and in imposing essential boundary conditions (EBC). Motivated by conventional finite volume methods, we propose a meshfree finite volume method (MFVM), where the trial functions are constructed through the conventional RKP or MLS procedures, while the test functions are set to be piecewise constants on Voronoi diagrams built on scattered particles. The proposed method possesses three typical merits: (1) the standard Gaussian rules are proven to produce optimal approximation errors; (2) the EBC can be imposed directly on boundary particles; and (3) mass conservation is maintained locally due to its finite volume formulations. Inf-sup conditions for the MFVM are proven in a one-dimensional problem, and are demonstrated numerically using a generalized eigenvalue problem for higher dimensions. Numerical test results are reported to verify the theoretical findings.

1. Introduction

We have seen extensive study of meshfree methods (also referred to as meshless methods) in the last decades and many significant developments have been achieved. A meshfree method (MM) establishes approximation functions using scattered particles to reduce the heavy computing load associated with the mesh generation in mesh-based methods (e.g., the finite element method (FEM)). The MM has been successfully applied to many engineering problems, especially those

* Corresponding author.
E-mail addresses: li@wayne.edu (H. Li), zhangqh6@mail.sysu.edu.cn (Q. Zhang).

[1] This research was partially supported by the NSF Grant DMS-1819041 and the Wayne State University Career Development Chair Award.
[2] This research was partially supported by the Natural Science Foundation of China under grant 11471343, 11628104, and 91730305, Guangdong Provincial Natural Science Foundation of China under grant 2015A030306016, and Fundamental Research Funds for Central Universities of China under grant 17lgzd28.

https://doi.org/10.1016/j.apnum.2020.02.005
0168-9274/

where the use of FEMs would require expensive remeshing of the domain, such as the problems with large deformations, crack propagation, impact dynamics, etc. We refer to [1,4,10,11,15,36,39] for various aspects on MMs. In this paper, we study the MM that is based on weak formulations and uses the shape functions that reproduce polynomials of degree k. Examples of such MMs include reproducing kernel particle methods (RKP) [30,39], moving least-square methods (MLS) [40], and meshless local Petrov-Galerkin methods (MLPG) [1–3].

It is well known that numerical integration and imposition of essential boundary conditions (EBC) lead to major difficulties in the MM. The MM becomes quite time-consuming and may even fail to simulate the actual problem if these difficulties are not addressed properly. First, the shape functions of MM are often not piecewise polynomials, and the conventional Gaussian integration rules cause notable integration errors. Many novel ideas have been proposed to improve the accuracy of the numerical integration, including background mesh integration [11,21,28,44], nodal integration [9,16,14,15,23], partition of unity quadrature [13], stress point integration [22,27], support integrations [6,44–46,38,43], and others [1,5,20]. However, the effect of the numerical integration on MMs has not been understood sufficiently well, and the theoretical analysis on the numerical integration is still in its early stages [5,6,44–46]. Second, the shape functions of MM do not satisfy the so-called Kronecker property. Therefore, it can be very difficult to impose EBC in the MM. The efforts to address the EBC can be categorized into the following classes: coupling with FEMs [34,25,31] and modifying bilinear forms, such as the penalty method [4,10,49], the Lagrange multiplier method [4,11], the Nitsche's method [4,25,29,33,41]. Various new approaches in this area can be found in [26,32,48]. The coupling with FEMs causes essential modifications of the current MM code framework, while modifying bilinear forms produces complicated bilinear forms and often introduces external parameters, such as penalty parameters and stability parameters, which are difficult to select in a unified approach. To the best of our knowledge, there has not been an MM that (1) uses the conventional Gaussian rules, (2) maintains the optimal convergence order $O(h^k)$ in the energy norm with numerical integration, and (3) imposes the EBC directly, where h is a discretization parameter.

We briefly analyze the difficulties before designing an MM that satisfies (1)–(3). An integration constraint condition was proposed in [6,45,46] as follows:

$$\fint_{\omega_i} \nabla p \cdot \nabla \psi_i \, dx + \fint_{\omega_i} \triangle p \, \psi_i \, dx - \fint_{\partial\omega_i} \frac{\partial p}{\partial n} \psi_i \, ds = 0, \quad \forall \ p \in \mathcal{P}_k, \tag{1.1}$$

where ψ_i is the shape function of the MM, $\mathcal{P}_k$ is the space of polynomials of degree k, $\fint_{\omega_i}$ and $\fint_{\partial\omega_i}$ are the numerical integrations for $\int_{\omega_i}$ and $\int_{\partial\omega_i}$, respectively. It is noted that the equality (1.1) holds automatically because of the Green formula if the numerical integration in (1.1) is exact. Based on (1.1), an approximation error $O(h^k + \eta h^{k-1})$ in the energy norm was proven in [6,45,46], where η is a constant representing the accuracy of the primary integration rule. After a detailed investigation on (1.1), we find that ψ_i in (1.1) is introduced as a test function rather than a trial function. The conventional Gaussian rules cannot make (1.1) hold because of the non-polynomial features of ψ_i. This is a major source of the integration errors in MMs. Meanwhile, the error $O(h^k + \eta h^{k-1})$ cannot be reduced by increasing the degree of polynomials in (1.1). Note that the supports of ψ_i's are overlapping, and the integration errors caused by different ψ_i cannot be canceled. Finally, the reason that it is difficult to impose the EBC in the MM is that the supports of the test functions ψ_i's, associated with the particles inside the domains (not on their boundaries), do not vanish on the domain boundary. This yields nonconforming integration terms on the essential boundary, and consequently direct imposition of EBC based on the standard bilinear forms can lead to large conforming errors.

According to the analysis above, it is important to take both the numerical integration and the EBC into account when designing a new MM. In particular, we would like to have an MM such that its test functions ψ_i's (a) satisfy (1.1) when the conventional Gaussian rules are applied, (b) have non-overlapping supports, and (c) vanish on the domain boundary for those associated with the particles inside the domain. Motivated by the finite volume method (FVM) [7,35,12,17,47,37], we propose a meshfree finite volume method (MFVM) in this study. The trial functions are produced by the conventional MMs, such as the RKP [30,39] and MLS [40]. The test functions are designed based on a Voronoi diagram constructed through the particles. Specifically, let D_i's be the sub-regions (control volumes associated with the particles) of the Voronoi diagram, as shown in Fig. 1. The test function ψ_i is chosen to be the indicator function $\mathbf{1}_{D_i}$ that is 1 in D_i and 0 outside D_i. It is easy to show that such D_i and $\psi_i = \mathbf{1}_{D_i}$ satisfy (a)–(c) above. Indeed, it is shown theoretically and numerically in this paper that the MFVM with the test function $\psi_i = \mathbf{1}_{D_i}$ satisfies (1)–(3). Namely, it produces the optimal convergence order $O(h^k)$ in the energy norm with the conventional Gaussian rules, and imposes the EBC directly at the nodes on the essential boundary. Moreover, as in the conventional FVM, the inclusion of the indicator function $\mathbf{1}_{D_i}$ in the test space ensures the mass conservation in each control volume D_i. It is clear that our MFVM is a Petrov-Galerkin method, like the conventional FVM. The inf-sup condition for the MFVM is proven in a one-dimensional problem, and a generalized eigenvalue problem is developed to numerically verify the inf-sup conditions in other dimensions. We stress that the Voronoi diagrams are essentially different from the FEM meshes that require certain conforming conditions, such as maximum angle or shape regular conditions [18]. The Voronoi diagrams can be established together with connectivity of the particles by mature algorithms [24]. The Voronoi diagrams were used in the MM to make nodal integration [16] as well as to propose virtual element methods [8] and natural element methods [42]. We mention that similar ideas were applied to fluid dynamics [19], as well as appeared in the MLPG 5 [1–3], where the supports of the test functions were overlapping and the EBCs were imposed by the penalty methods. Moreover, the optimal convergence with the numerical integration was not proven there.

The paper is organized as follows. In Section 2, we introduce the model problem and describe the MFVM. The inf-sup conditions of the MFVM are studied in Section 3. The effect of numerical integration on the MFVM is analyzed in Section 4, where the conventional Gaussian rules are shown to ensure the MFVM to converge with the optimal order $O(h^k)$ in the energy norm. In Section 5, the direct imposition of EBC is presented for the MFVM, and the optimal convergence is proven theoretically. Numerical tests are presented in Section 6 to demonstrate efficiency of the proposed algorithm and to verify theoretical results. Concluding remarks are included in Section 7.

2. The model problem and the MFVM

Let D be a domain in $\mathbb{R}^d$ $(1 \le d \le 3)$ and $m \ge 0$ be an integer, and let $1 \le p \le +\infty$. We denote the usual Sobolev space as $W^{m,p}(D)$ with norm $\|\cdot\|_{W^{m,p}(D)}$ and semi-norm $|\cdot|_{W^{m,p}(D)}$. The space $W^{m,p}(D)$ will be represented by $H^m(D)$ in the case $p = 2$ and $L^p(D)$ when $m = 0$, respectively. We denote by $H_0^m(D)$ the set of all functions in $H^m(D)$ having zero values at the boundary ∂D. The polynomial space of degree k in $\mathbb{R}^d$ is denoted by $\mathcal{P}_k$.

Let $\Omega \subset \mathbb{R}^d$ be a bounded domain with a Lipschitz boundary $\Gamma := \partial\Omega$. To better present the idea, we first consider a model problem with the Neumann boundary condition

$$\begin{aligned} -\triangle u &= f, \quad \text{in } \Omega \\ \nabla u \cdot \vec{n} &= g, \quad \text{on } \Gamma, \end{aligned} \tag{2.1}$$

where $\vec{n}$ is the unit outward normal vector to Γ, $f \in L^2(\Omega)$, $g \in L^2(\Gamma)$, and the solution u to (2.1) is assumed to satisfy $u \in W^{k+1,\infty}(\Omega)$. The essential boundary conditions (EBC) will be addressed specifically in Section 5.

An equivalent variational formulation solving (2.1) is given by

$$\text{Find } u \in H^1(\Omega) \text{ such that } B(u, v) = F(v), \ \forall\, v \in H^1(\Omega), \tag{2.2}$$

where

$$B(u, v) \equiv \int_\Omega \nabla u \cdot \nabla v \, dx, \quad F(v) \equiv \int_\Omega f\, v \, dx + \int_\Gamma g\, v \, ds.$$

The approximation space in the MM

The meshfree methods (MMs), such as the reproducing kernel particle methods (RKP), the moving least-square methods (MLS), and the meshless local Petrov-Galerkin methods (MLPG), approximate the variational problem (2.2) using scattered particles in Ω instead of meshes in mesh-based methods (e.g., the FEM). Let $X_h = \{x_i,\, i \in N_h\} \subset \bar{\Omega}$ be the set of particles, represented by a small discretization parameter h, where N_h is an index set. Let $U_h = \text{span}\{\phi_i : i \in N_h\}$ be a family of finite-dimensional subspaces, where each ϕ_i is associated with a particle x_i. The shape functions ϕ_i's are compactly supported, and denote $\omega_i \equiv \overline{\text{supp}\,\phi_i}$ and $h_i \equiv \text{diam}\,\omega_i$. We divide N_h into two parts: $N_h' = \{i \in N_h : x_i \in \Gamma\}$ and $N_h'' = N_h \backslash N_h'$. The fundamental assumptions on U_h are as follows.

A1: We assume that the distribution of the particles is quasi-uniform, i.e., there exist positive constants C_1 and C_2, independent of h and i, such that

$$C_1 \le \frac{h_i}{h} \le C_2 \ \text{ and } \ C_1 h^d \le |\omega_i| \le C_2 h^d, \tag{2.3}$$

where $|\omega_i|$ is the "area" of ω_i in $\mathbb{R}^d$.

A2: (Finitely overlapping) For $i \in N_h$, let $S_i \equiv \{j \in N_h : \omega_i \cap \omega_j \neq \emptyset\}$ and assume that there is a constant κ, independent of i, j, and h, such that

$$\text{card}\, S_i \le \kappa, \quad \forall\, i \in N_h. \tag{2.4}$$

A3: (Polynomials reproducing) The shape functions *reproduce polynomials of degree* k, i.e.,

$$\sum_{i \in N_h} p(x_i)\phi_i(x) = p(x), \quad \forall\, p \in \mathcal{P}^k \text{ and } x \in \Omega. \tag{2.5}$$

A4: There exists a positive constant C, independent of i and h, such that

$$\|D^\alpha \phi_i\|_{L^\infty(\omega_i)} \le C h_i^{-|\alpha|} \text{ for } |\alpha| = 0, 1, \ \alpha \text{ is a multi-index.} \tag{2.6}$$

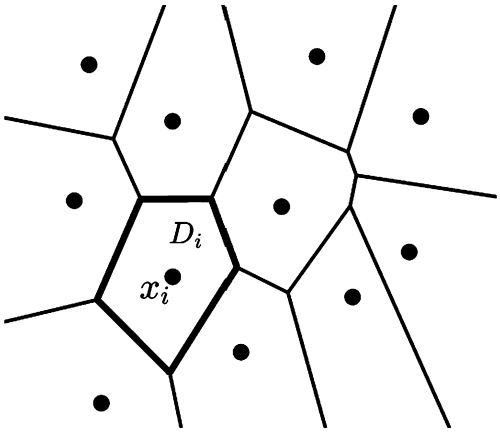

Fig. 1. An example on Voronoi diagram: D_i is the region associated with particle x_i.

A5: There exist positive constants C_1, C_2, independent of h and i, such that for any $i \in N_h$,

$$C_1\|v\|^2_{L^2(\omega_i)} \le h_i^d \sum_{j\in S_i} v_j^2 \le C_2\|v\|^2_{L^2(\omega_i)}, \tag{2.7}$$

$$C_1\|v\|^2_{L^2(\omega_i\cap\Gamma)} \le h_i^{d-1} \sum_{j\in S_i} v_j^2 \le C_2\|v\|^2_{L^2(\omega_i\cap\Gamma)}, \tag{2.8}$$

$$C_1|v|^2_{H^1(\omega_i)} \le h_i^{d-2} \sum_{j\in S_i} (v_j - v_i)^2 \le C_2|v|^2_{H^1(\omega_i)}, \tag{2.9}$$

where $v \in U_h$ is of the form $v = \sum_{i\in N_h} v_i \phi_i$.

Remark 2.1. The subspace U_h that satisfies the assumptions **A1** – **A5** has been studied extensively. We refer to [4–6,46,30,40] for details. The approximation properties of U_h are also well known in the literature. We present the following approximation property that will be employed in this paper, and its proof could be found in [4,30,40,46]. For $u \in W^{k+1,\infty}(\Omega)$, define the U_h-interpolant of u by $\mathcal{I}_h u$ as

$$\mathcal{I}_h u := \sum_{i\in I_h} u(x_i)\phi_i.$$

Lemma 2.1. *For any $u \in W^{k+1,\infty}(\Omega)$,*

$$\|u - \mathcal{I}_h u\|_{W^{l,\infty}(\Omega)} \le Ch^{k+1-l}|u|_{W^{k+1,\infty}(\Omega)}, \quad l = 0, 1, \cdots, k+1, \tag{2.10}$$

where C is a constant independent of h and u.

■

A Galerkin meshfree method to discretize (2.2) is given by

$$\text{Find } \vartheta_h \in U_h \text{ such that } B(\vartheta_h, v_h) = F(v_h), \ \forall\, v_h \in U_h. \tag{2.11}$$

Using a standard Céa lemma and (2.10), we have

$$|u - \vartheta_h|_{H^1(\Omega)} \le C \inf_{v_h\in U_h} |u - v_h|_{H^1(\Omega)} \le C|u - \mathcal{I}_h u|_{H^1(\Omega)} \le Ch^k|u|_{W^{k+1,\infty}(\Omega)}.$$

A meshfree finite volume method

It is well known that the Galerkin meshfree methods (2.11) based on **A1**–**A5** can be less effective due to numerical integration and imposition of the EBC (see Introduction). In what follows, we propose a meshfree finite volume method (MFVM) that maintains the mass conservation as the conventional FVMs, and also addresses the concerns in numerical integration and in the EBC.

Let $D_i, i \in N_h$, be regions of the Voronoi diagram constructed from the particles X_h, where D_i is associated with particle x_i (see Fig. 1). D_i is called a *control volume* with respect to x_i. Define $\mathbf{1}_{D_i}$ to be the indicator function on D_i that is 1 in

D_i and 0 outside D_i, and $V_h = \text{span}\{\mathbf{1}_{D_i} :, i \in N_h\}$. It is obvious that $\dim(U_h) = \dim(V_h)$. Multiplying $\mathbf{1}_{D_i}$ on both sides of (2.1) and making integration by part yields

$$-\int_{\partial D_i \setminus \Gamma} \nabla u \cdot \vec{n}_i ds = \int_{D_i} f(x)dx + \int_{\partial D_i \cap \Gamma} g(s)ds, \ \ \forall\ i \in N_h, \tag{2.12}$$

where $\vec{n}_i$ is the unit outward normal vector to the boundary of D_i. According to (2.12), we define a bilinear form A_h on $H^1(\Omega) \times V_h$

$$A_h(v, \sigma_h) := \sum_{i \in N_h} c_i \left(-\int_{\partial D_i \setminus \Gamma} \nabla v \cdot \vec{n}_i ds \right), \ \ \forall\ v \in H^1(\Omega) \text{ and } \forall\ \sigma_h = \sum_{i \in N_h} c_i \mathbf{1}_{D_i}$$

and a linear functional L_h on V_h

$$L_h(\sigma_h) := \sum_{i \in N_h} c_i \left(\int_{D_i} f(x)dx + \int_{\partial D_i \cap \Gamma} g(s)ds \right), \ \ \forall\ \sigma_h = \sum_{i \in N_h} c_i \mathbf{1}_{D_i}.$$

Hence, (2.12) becomes

$$A_h(u, \sigma_h) = L(\sigma_h), \ \ \forall\ \sigma_h \in V_h. \tag{2.13}$$

The MFVM to discretize (2.13) is defined as follows:

$$\text{Find } u_h \in U_h \ \text{ such that } \ A_h(u_h, \sigma_h) = L(\sigma_h), \ \ \forall\ \sigma_h \in V_h. \tag{2.14}$$

We refer to U_h and V_h as the trial and test spaces of the MFVM, respectively. Note that the inclusion of indicator functions $\mathbf{1}_{D_i}$ on control volumes in the test space is to ensure the mass conservation on each control volume D_i.

Recall $\dim(U_h) = \dim(V_h)$. For simplicity, we define a one-to-one mapping which maps a trial function $w_h = \sum_{j \in N_h} w_j \phi_j \in U_h$ to a test function $w_h^* \in V_h$ by

$$w_h^* = \left(\sum_{j \in N_h} w_j \phi_j \right)^* = \sum_{j \in N_h} w_j \mathbf{1}_{D_j} \in V_h.$$

With this mapping, the MFVM (2.14) can be rewritten as a variational formulation on U_h as follows

$$\text{Find } u_h \in U_h \ \text{ such that } \ A_h^*(u_h, w_h) = L_h^*(w_h), \ \ \forall\ w_h \in U_h, \tag{2.15}$$

where A_h^* is a bilinear form on $H^1(\Omega) \times U_h$, and L_h^* a linear functional on U_h, defined by

$$A_h^*(v, w_h) := A_h(v, w_h^*) \text{ and } L_h^*(w_h) := L_h(w_h^*), \ \ \forall\ v \in H^1(\Omega), \ \ w_h \in U_h.$$

We next prove a continuity result for A_h^*.

Lemma 2.2. *A_h^* is continuous on $H^2(\Omega) \times U_h$, namely, there exists a constant C independent of h and $i \in N_h$ such that*

$$\left| A_h^*(v, w_h) \right| \le C(|v|_{H^1(\Omega)} + h|v|_{H^2(\Omega)})|w_h|_{H^1(\Omega)}, \ \ \forall\ v \in H^2(\Omega), \ \ w_h \in U_h. \tag{2.16}$$

Proof. Let $w_h = \sum_{i \in N_i} w_i \phi_i$. Then

$$A_h^*(v, w_h) = \sum_{i \in N_h} w_i \left(-\int_{\partial D_i \setminus \Gamma} \nabla v \cdot \vec{n}_i ds \right) = \frac{1}{2} \sum_{i \in N_h} \left(\sum_{j \in \check{S}_i} (w_j - w_i) \int_{\partial D_{i,j}} \nabla v \cdot \vec{n}_{i,j} ds \right), \tag{2.17}$$

where $\check{S}_i = \{j \in N_h : (\partial D_j \setminus \Gamma) \cap (\partial D_i \setminus \Gamma) \neq \emptyset\}$, $\partial D_{i,j} = (\partial D_j \setminus \Gamma) \cap (\partial D_i \setminus \Gamma)$, and $\vec{n}_{i,j}$ is a unit vector normal to $\partial D_{i,j}$ and directed toward D_j. Using the Cauchy-Schwarz inequality in (2.17) produces

$$|A_h^*(v,w_h)| \le \frac{1}{2}\sum_{i\in N_h}\left(\sum_{j\in\check{S}_i}(w_j-w_i)^2\right)^{1/2}\left(\sum_{j\in\check{S}_i}\Big(\int_{\partial D_{i,j}}\nabla v\cdot\vec{n}_{i,j}ds\Big)^2\right)^{1/2},$$

$$\le C\left(\sum_{i\in N_h}\Big(\sum_{j\in\check{S}_i}(w_j-w_i)^2\Big)\right)^{1/2}\left(\sum_{i\in N_h}\Big(\sum_{j\in\check{S}_i}h^{d-1}\int_{\partial D_{i,j}}|\nabla v\cdot\vec{n}_{i,j}|^2ds\Big)\right)^{1/2},$$

$$\le Ch^{1-\frac{d}{2}}|w_h|_{H^1(\Omega)}h^{\frac{d-1}{2}}\left(\sum_{i\in N_h}\int_{\partial D_i\setminus\Gamma}|\nabla v\cdot\vec{n}_i|^2ds\right)^{1/2},$$

where the last inequality is because of (2.9). Finally, according to the trace inequality, we have

$$|A_h^*(v,w_h)| \le Ch^{\frac{1}{2}}|w_h|_{H^1(\Omega)}\left(\frac{1}{h}\sum_{i\in N_h}\Big(|v|^2_{H^1(D_i)}+h^2|v|^2_{H^2(D_i)}\Big)\right)^{1/2} = C|w_h|_{H^1(\Omega)}(|v|_{H^1(\Omega)}+h|v|_{H^2(\Omega)}),$$

which is the desired result. □

It is noted that A_h^* is not symmetric on U_h. Thus, the inf-sup condition of bilinear form A_h^* in U_h is crucial for success of the MFVM. We formulate the inf-sup condition as an assumption for now and shall investigate it further in the next sections.

Assumption. (inf-sup condition) There exists a constant $\alpha > 0$ independent of i and h such that for any $v_h \in U_h$, there is $w_h \in U_h$ satisfying

$$A_h^*(v_h,w_h) \ge \alpha|v_h|_{H^1(\Omega)}|w_h|_{H^1(\Omega)}. \tag{2.18}$$

Remark 2.2. We will prove the inf-sup condition (2.18) of A_h^* for the one-dimensional case in the next section. For general cases, we will present a generalized eigenvalue approach to verify the inf-sup condition (2.18) numerically.

Theorem 2.1. *Let $u \in H^2(\Omega)$ be the solution to (2.1), and assume the bilinear form A_h^* satisfies the inf-sup condition (2.18) on U_h, then the MFVM scheme (2.15) (or (2.14)) has a unique solution u_h satisfying*

$$|u-u_h|_{H^1(\Omega)} \le C\inf_{w_h\in U_h}(|u-w_h|_{H^1(\Omega)}+h|u-w_h|_{H^2(\Omega)}). \tag{2.19}$$

Proof. For all $v_h \in U_h$, we have

$$A_h^*(u_h,v_h) = L^*(v_h) = A_h^*(u,v_h), \text{ and } A_h^*(u-u_h,v_h) = 0.$$

Therefore, by (2.18) and (2.16), we have

$$|u_h-w_h|_{H^1(\Omega)} \le \frac{1}{\alpha}\sup_{v_h\in U_h}\frac{|A_h^*(u_h-w_h,v_h)|}{|v_h|_{H^1(\Omega)}} = \frac{1}{\alpha}\sup_{v_h\in U_h}\frac{|A_h^*(u-w_h,v_h)|}{|v_h|_{H^1(\Omega)}}$$

$$\le \frac{C}{\alpha}(|u-w_h|_{H^1(\Omega)}+h|u-w_h|_{H^2(\Omega)}),$$

from which (2.19) follows immediately since $|u-u_h|_{H^1(\Omega)} \le |u-w_h|_{H^1(\Omega)}+|u_h-w_h|_{H^1(\Omega)}$. □

Remark 2.3. The result (2.19) means that the MFVM solution reaches the optimal convergence under the assumption (2.18). We refer to [4,30,40] for the approximation properties of the trial space U_h.

Remark 2.4. The solution to (2.15) is unique up to a constant since we solve a pure Neumann problem (2.1). There are several conventional approaches to ensure a unique solution to (2.15), such as Lagrange multiplier and imposing zero value at a particular point in Ω, see [6] in detail. We use the latter in this paper for convenience to present the main idea. Let $z_0 \in \Omega$ be fixed, and we solve (2.15) under a constraint $u_h(z_0) = 0$ to ensure a unique solution. This approach will be used for the pure Neumann problems in other sections without describing it specifically.

3. The inf-sup condition

We prove the inf-sup condition (2.18) for a one-dimensional case. A generalized eigenvalue problem is proposed to numerically verify the inf-sup condition (2.18) in two- and three-dimensions.

Let $\Omega = (0,1)$, and suppose N particles $\{x_i : i = 1, \cdots, N\}$ with $x_1 = 0, x_N = 1$ are scattered in $\bar{\Omega}$. We assume that x_i are quasi-uniformly distributed, and h_i are set so that the shape function ϕ_i satisfies the assumption **A1** − **A5** with $k = 1$. It is clear that in this case the associated Voronoi diagram consists of sub-intervals $[\bar{x}_{i-1}, \bar{x}_i]$, $i = 1, 2, \cdots, N$, where $\bar{x}_i = \frac{1}{2}(x_i + x_{i+1})$, $i = 1, 2, \cdots N-1$, and $\bar{x}_0 = x_1, \bar{x}_N = x_N$. Therefore, the test space V_h is given by

$$V_h = \text{span}\{\mathbf{1}_{[\bar{x}_{i-1}, \bar{x}_i]} : i = 1, 2, \cdots, N\}.$$

To simplify the presentation, we assume that the support diameter h_i are chosen such that each $\bar{x}_i$ is covered by the supports of two shape functions ϕ_i and ϕ_{i+1}. We mention that it is not a serious restriction since we are considering the linear polynomial reproducing ((2.5) with $k = 1$).

Proposition 3.1. *Assume that the shape function ϕ_i's satisfy the assumptions* **A1** − **A5** *with $k = 1$, and each $\bar{x}_i$ is covered by supports of two shape functions ϕ_i and ϕ_{i+1}. Then there is constant C independent of h and i such that*

$$A_h^*(u_h, u_h) \geq C|u_h|^2_{H^1(\Omega)}, \quad \forall\ u_h \in U_h. \tag{3.1}$$

Proof. For $u_h = \sum_{i=1}^N c_i \phi_i \in U_h$, we have

$$A_h^*(u_h, u_h) = -c_1 u_h'(\bar{x}_1) + \sum_{i=2}^{N-1} c_i (u_h'(\bar{x}_{i-1}) - u_h'(\bar{x}_i)) + c_N u_h'(\bar{x}_{N-1}) = \sum_{i=1}^{N-1} u_h'(\bar{x}_i)(c_{i+1} - c_i). \tag{3.2}$$

Since $\bar{x}_i$ is covered by the supports of two shape functions ϕ_i and ϕ_{i+1}, we have

$$u_h'(\bar{x}_i) = c_i \phi_i'(\bar{x}_i) + c_{i+1}\phi_{i+1}'(\bar{x}_i) = \phi_{i+1}'(\bar{x}_i)(c_{i+1} - c_i). \tag{3.3}$$

We obtain (3.3) due to the reproducing property (2.5) that gives

$$\phi_i(\bar{x}_i) + \phi_{i+1}(\bar{x}_i) = 1 \ \text{ and } \ \phi_i'(\bar{x}_i) + \phi_{i+1}'(\bar{x}_i) = 0.$$

With (3.2) and (3.3), we have

$$A_h^*(u_h, u_h) = \sum_{i=1}^{N-1} \phi_{i+1}'(\bar{x}_i)(c_{i+1} - c_i)^2. \tag{3.4}$$

The particles x_i are quasi-uniformly distributed. Then there is a constant C independent of h and i such that $|x_{i+1} - \bar{x}_i| \geq Ch$ ($\bar{x}_i$ is the center of $[x_i, x_{i+1}]$), which yields that

$$C_1 \frac{1}{h} \leq \phi_{j+1}'(\bar{x}_j) \leq C_2 \frac{1}{h},$$

where C_1, C_2 are constants independent of h and i. Therefore, we have

$$A_h^*(u_h, u_h) \geq \sum_{i=1}^{N-1} C \frac{1}{h}(c_{i+1} - c_i)^2 \geq C|u_h|^2_{H^1(\Omega)},$$

where the last inequality comes from (2.9). □

In fact, we have derived a stronger result (3.1) in a special one-dimensional case, which leads to the inf-sup condition (2.18) directly. The condition (3.1) is referred to as the coercivity of A_h^*. Meanwhile, the inf-sup condition (2.18) can be verified numerically for higher dimensions and higher degrees k of reproducing polynomials, as shown in the numerical experiments. We shall present a generalized eigenvalue problem to verify the inf-sup numerically in general situations.

To this end, we denote by $\mathbf{A}$ the stiffness matrix derived from (2.15). We also need the stiffness matrix $\mathbf{B}$ from the Galerkin method based on the bilinear form $B(\cdot,\cdot)$ on U_h (see (2.2)). It is noted that $\mathbf{A}$ is not symmetric, and $\mathbf{B}$ is symmetric. For arbitrary $u_h = \sum_i u_i \phi_i$ and $v_h = \sum v_i \phi_i$ in U_h, we denote by $\mathbf{u} = [u_i]$ and $\mathbf{v} = [v_i]$ the coefficient vectors of u_h and v_h. Therefore, the inf-sup condition (2.18) has the equivalent matrix-vector form

$$\inf_{\mathbf{u} \in \mathbb{R}^N} \sup_{\mathbf{v} \in \mathbb{R}^N} \frac{\mathbf{v}^T \mathbf{A} \mathbf{u}}{\sqrt{\mathbf{u}^T \mathbf{B} \mathbf{u}} \sqrt{\mathbf{v}^T \mathbf{B} \mathbf{v}}} > \alpha. \tag{3.5}$$

Let $\mathbf{w} = \mathbf{B}^{\frac{1}{2}}\mathbf{v}$, we have from (3.5)

$$\alpha < \inf_{\mathbf{u}\in\mathbb{R}^N} \sup_{\mathbf{w}\in\mathbb{R}^N} \frac{\mathbf{w}^T\mathbf{B}^{-\frac{1}{2}}\mathbf{A}\mathbf{u}}{\sqrt{\mathbf{u}^T\mathbf{B}\mathbf{u}}\|\mathbf{w}\|} = \inf_{\mathbf{u}\in\mathbb{R}^N} \frac{\|\mathbf{B}^{-\frac{1}{2}}\mathbf{A}\mathbf{u}\|}{\sqrt{\mathbf{u}^T\mathbf{B}\mathbf{u}}} = \inf_{\mathbf{u}\in\mathbb{R}^N} \sqrt{\frac{\mathbf{u}^T\mathbf{A}^T\mathbf{B}^{-1}\mathbf{A}\mathbf{u}}{\mathbf{u}^T\mathbf{B}\mathbf{u}}}, \tag{3.6}$$

namely,

$$\mathbf{u}^T\mathbf{A}^T\mathbf{B}^{-1}\mathbf{A}\mathbf{u} > \alpha^2\mathbf{u}^T\mathbf{B}\mathbf{u}, \ \forall\, \mathbf{u}\in\mathbb{R}^N.$$

It is clear that α^2 can be bounded below by the smallest eigenvalue $\lambda_{\min}$ of a generalized eigenvalue problem

$$\mathbf{A}^T\mathbf{B}^{-1}\mathbf{A}\mathbf{u} = \lambda\mathbf{B}\mathbf{u}. \tag{3.7}$$

We refer to $\lambda_{IS} := \sqrt{\lambda_{\min}}$ as the inf-sup constant of the MFVM, which will be employed to verify the inf-sup conditions for the MFVM numerically when h is not very small. Numerical test results will be presented in Section 6.

4. Effect of numerical integration

Numerical integration plays an important role in effective implementation of meshless methods, largely due to the non-polynomial features of the shape functions. In [6,45,46], a novel integration rule was developed where the integration formulations were required to satisfy the discrete Green formula (1.1); consequently, the approximation error in the energy norm was bounded by $O(h^k + \eta h^{k-1})$, where η is a constant representing the accuracy of the primary integration rules. This error estimate is sub-optimal and the standard Gaussian rules do not satisfy (1.1) because of the non-polynomial features of ψ_i. Note that ψ_i is introduced in (1.1) as the test function rather than the trial function. Therefore, if the test function ψ_i is the piecewise constant $\mathbf{1}_{D_i}$, similar to the case in the MFVM, equation (1.1) will hold for the standard Gaussian rules. This, along with the disjoint supports of $\mathbf{1}_{D_i}$, enables us to improve the sub-optimal error estimate $O(h^k + \eta h^{k-1})$ to an optimal estimate $O(h^k)$. The detailed analysis on the effect of numerical integration on the proposed MFVM will be carried out in this section.

We consider the proposed MFVM (2.15) and let $u_h = \sum_{j\in N_h} c_j\phi_j$ be its solution. Then we obtain a linear system from the discretized variational formulation (2.15)

$$\sum_{j\in N_h} \beta_{ij}c_j = l_i, \ \forall\, i\in N_h, \tag{4.1}$$

where

$$\beta_{ij} \equiv A_h^*(\phi_j,\phi_i) = -\int_{\partial D_i\setminus\Gamma} \nabla\phi_j\cdot\vec{n}_i ds \ \text{ and } \ l_i \equiv L^*(\phi_i) = \int_{D_i} f dx + \int_{\partial D_i\cap\Gamma} g(s)ds.$$

In practice, these integration terms are computed numerically as follows:

$$\tilde{\beta}_{ij} \equiv -\fint_{\partial D_i\setminus\Gamma} \nabla\phi_j\cdot\vec{n}_i ds \ \text{ and } \ \tilde{l}_i \equiv \fint_{D_i} f dx + \fint_{\partial D_i\cap\Gamma} g(s)ds,$$

where $f_{\partial D_i\setminus\Gamma}$, f_{D_i}, $f_{\partial D_i\cap\Gamma}$ are the numerical integration in the stiffness matrix $[\tilde{\beta}_{ij}]$ and the load vector $[\tilde{l}_i]$, respectively. We in fact will solve a version of system (4.1) with numerical integration:

$$\sum_{j\in N_h} \tilde{\beta}_{ij}c_j = \tilde{l}_i, \ \forall\, i\in N_h. \tag{4.2}$$

To analyze the approximation error of solution to (4.2), we develop an equivalent operator form of (4.2). For any u_h and w_h in U_h with expressions $\sum_{j\in N_h} u_j\phi_j$ and $\sum_{i\in N_h} w_i\phi_i$, respectively, we define

$$\tilde{A}_h^*(u_h,w_h) \equiv \sum_{i,j\in N_h} u_j\tilde{\beta}_{ij}w_i \ \text{ and } \ \tilde{L}^*(w_h) \equiv \sum_{i\in N_h} w_i\tilde{l}_i, \tag{4.3}$$

which are a bilinear form and a linear functional on U_h, respectively. Then the linear system (4.2) is equivalent to

$$\text{Find } \tilde{u}_h\in U_h \text{ such that } \tilde{A}_h^*(\tilde{u}_h,w_h) = \tilde{L}^*(w_h), \quad \forall\, w_h\in U_h. \tag{4.4}$$

To establish the unique solvability of (4.4), we prove the inf-sup condition of bilinear form $\tilde{A}_h^*$ on U_h. To this end, the following result will be used below, i.e., there exists a small positive constant τ, independent of h, i, and j, such that for each $i, j\in N_h$

$$\Big| \int\limits_{\partial D_i\setminus\Gamma} \nabla\phi_j ds - \fint\limits_{\partial D_i\setminus\Gamma} \nabla\phi_j ds \Big| \le \tau |\partial D_i\setminus\Gamma| \, \|\nabla\phi_i\|_{L_\infty(\Omega_{ij})}, \tag{4.5}$$

where τ is associated with accuracy of the integration rule $f_{\partial D_i\setminus\Gamma}$ and decreases as the integration accuracy increases. The proof of (4.5) can be found out in [44,6].

Proposition 4.1. *(inf-sup) There exists a constant $\tilde{\alpha}$ independent of i and h such that for any $v_h \in U_h$, there is a $w_h \in U_h$ satisfying*

$$\tilde{A}_h^*(v_h, w_h) \ge \tilde{\alpha} |v_h|_{H^1(\Omega)} |w_h|_{H^1(\Omega)}. \tag{4.6}$$

Proof. According to the inf-sup condition (2.18) of A_h^*, for any $v_h \in U_h$, there is a $w_h \in U_h$ satisfying

$$A_h^*(v_h, w_h) \ge \alpha |v_h|_{H^1(\Omega)} |w_h|_{H^1(\Omega)}. \tag{4.7}$$

We next estimate difference between $A_h^*(v_h, w_h)$ and $\tilde{A}_h^*(v_h, w_h)$. Let $v_h = \sum_{i\in N_i} v_i\phi_i$ and $w_h = \sum_{i\in N_i} w_i\phi_i$. Using the similar calculation with (2.17) and the Cauchy-Schwarz inequality, we have

$$\begin{aligned} \Big| A_h^*(v_h, w_h) - \tilde{A}_h^*(v_h, w_h) \Big| &= \Big| \sum_{i\in N_h} w_i \left(\Big[\fint\limits_{\partial D_i\setminus\Gamma} - \int\limits_{\partial D_i\setminus\Gamma} \Big] \nabla v_h \cdot \vec{n}_i ds \right) \Big| \\ &= \Big| \frac{1}{2} \sum_{i\in N_h} \left(\sum_{j\in \check{S}_i} (w_j - w_i) \Big(\Big[\int\limits_{\partial D_{i,j}} - \fint\limits_{\partial D_{i,j}} \Big] \nabla v_h \cdot \vec{n}_{i,j} ds \Big) \right) \Big| \\ &\le \frac{1}{2} \left(\sum_{i\in N_h} \sum_{j\in \check{S}_i} (w_j - w_i)^2 \right)^{1/2} \left(\sum_{i\in N_h} \sum_{j\in \check{S}_i} \Big(\Big[\int\limits_{\partial D_{i,j}} - \fint\limits_{\partial D_{i,j}} \Big] \nabla v_h \cdot \vec{n}_{i,j} ds \Big)^2 \right)^{1/2} =: \frac{1}{2} I_1 \times I_2. \end{aligned} \tag{4.8}$$

It is proven in Lemma 2.2

$$I_1 \le C h^{1-\frac{d}{2}} |w_h|_{H^1(\Omega)}. \tag{4.9}$$

We next estimate I_2. For any $i \in N_h$ and $j \in \check{S}_i$, we have

$$\begin{aligned} \Big| \Big[\int\limits_{\partial D_{i,j}} - \fint\limits_{\partial D_{i,j}} \Big] \nabla v_h \cdot \vec{n}_{i,j} ds \Big|^2 &= \left| \Big[\int\limits_{\partial D_{i,j}} - \fint\limits_{\partial D_{i,j}} \Big] \sum_{l\in S_i} (v_l - v_i) \nabla\phi_l \cdot \vec{n}_{i,j} ds \right|^2 \\ &= \left| \sum_{l\in S_i} (v_l - v_i) \Big[\int\limits_{\partial D_{i,j}} - \fint\limits_{\partial D_{i,j}} \Big] \nabla\phi_l \cdot \vec{n}_{i,j} ds \right|^2 \\ &\le \left(\sum_{l\in S_i} (v_l - v_i)^2 \right) \left(\sum_{l\in S_i} \left(\Big[\int\limits_{\partial D_{i,j}} \nabla\phi_l ds - \fint\limits_{\partial D_{i,j}} \nabla\phi_l ds \Big] \cdot \vec{n}_{i,j} \right)^2 \right) \\ &\le C h^{2-d} |v_h|^2_{H^1(\omega_i)} (\mathrm{Card}\, S_i) \tau^2 |\partial D_i \setminus \Gamma|^2 \|\nabla\phi_i\|^2_{L_\infty(\Omega_{ij})} \\ &\le C h^{2-d} |v_h|^2_{H^1(\omega_i)} \kappa \tau^2 h^{2d-2} h^{-2}, \end{aligned} \tag{4.10}$$

where we use (2.9), (4.5), (2.4), and (2.6) to get the last two inequalities. Then, using (4.10) in (4.8) and noting $\mathrm{Card}\, \check{S}_i \le \mathrm{Card}\, S_i \le \kappa$, we get

$$I_2 \le \left(C \sum_{i\in N_h} (\mathrm{Card}\, \check{S}_i) \kappa \tau^2 h^{d-2} |v_h|^2_{H^1(\omega_i)} \right)^{1/2} \le C\kappa\tau h^{\frac{d}{2}-1} \left(\sum_{i\in N_h} |v_h|^2_{H^1(\omega_i)} \right)^{1/2} \le C\kappa\tau h^{d-\frac{1}{2}} |v_h|_{H^1(\Omega)}.$$

Employing the estimates about I_2 and I_1 (4.9) in (4.8) yields

$$\left|A_h^*(v_h, w_h) - \tilde{A}_h^*(v_h, w_h)\right| \le C\tau |v_h|_{H^1(\Omega)} |w_h|_{H^1(\Omega)}.$$

Finally, $\tilde{A}_h^*(v_h, w_h) \ge A_h^*(v_h, w_h) - \left|A_h^*(v_h, w_h) - \tilde{A}_h^*(v_h, w_h)\right| \ge (\alpha - C\tau)|v_h|_{H^1(\Omega)} |w_h|_{H^1(\Omega)}$. We get the desired result by letting $\tilde{\alpha} = \alpha - C\tau$, which is large than 0 for small τ (τ decreases as the integration accuracy increases). □

With the inf-sup condition (4.6), the variational problem (4.4), perturbed by numerical integration, can be solved uniquely. We next analyze the optimal approximation errors of $\tilde{u}_h$.

Theorem 4.1. *Let u and $\tilde{u}_h$ be the solutions to (2.1) and (4.4), respectively. Suppose $u \in W^{k+1,\infty}(\Omega)$ and $f \in W^{k,\infty}(\Omega)$. Assume that for any $i \in N_h$ the numerical integration rules $\int_{\partial D_{i,j}}$, $j \in \check{S}_i$ and $\int_{D_i}$ are exact for polynomials of degree $k-1$ on $\partial D_{i,j}$ and D_i, respectively. Assume for any $i \in N_h'$, $\int_{D_i \cap \Gamma}$ is exact for polynomials of degree $k-1$ on $D_i \cap \Gamma$. Then there exists a constant C independent of h and i such that*

$$|u - \tilde{u}_h|_{H^1(\Omega)} \le Ch^k |u|_{W^{k+1,\infty}(\Omega)} + Ch^k |f|_{W^{k,\infty}(\Omega)}. \tag{4.11}$$

Proof. Let $\mathcal{I}_h u$ be the U_h-interpolant of u. We first present a Strang lemma as follows:

$$|\tilde{u}_h - \mathcal{I}_h u|_{H^1(\Omega)} \le C|u - \mathcal{I}_h u|_{H^1(\Omega)} + C \sup_{w_h \in U_h} \frac{|A_h^*(\mathcal{I}_h u, w_h) - \tilde{A}_h^*(\mathcal{I}_h u, w_h) + L_h^*(w_h) - \tilde{L}_h^*(w_h)|}{|w_h|_{H^1(\Omega)}}, \tag{4.12}$$

which can be proven in similar ways as in [6], and therefore we omit detailed calculations here. The second term in the right hand side of (4.12) is referred to as the conforming error of the numerical integration.

For a function $v \in W^{k+1,\infty}(\Omega)$, the Taylor polynomial of degree k of u evaluated at x_i is denoted by

$$T_i^k v(x) = \sum_{|\alpha| \le k} \frac{1}{\alpha!} D^\alpha v(x_i)(x - x_i)^\alpha.$$

A standard error estimate is known as follows:

$$|v - T_i^k v|_{W^{l,\infty}(D_i)} \le Ch^{k+1-l} |v|_{W^{k+1,\infty}(\Omega)}, \ l = 0, 1, \cdots, k+1. \tag{4.13}$$

According to (2.10) we have

$$\|\mathcal{I}_h u\|_{W^{k+1,\infty}(\Omega)} \le \|u\|_{W^{k+1,\infty}(\Omega)} + \|u - \mathcal{I}_h u\|_{W^{k+1,\infty}(\Omega)} \le C|u|_{W^{k+1,\infty}(\Omega)}. \tag{4.14}$$

Letting $w_h = \sum_{i \in N_h} w_i \phi_i$ and using the same calculation as (2.17), we have

$$|A_h^*(\mathcal{I}_h u, w_h) - \tilde{A}_h^*(\mathcal{I}_h u, w_h)| = \frac{1}{2} \sum_{i \in N_h} \left| \sum_{j \in \check{S}_i} (w_j - w_i) \Big[\int_{\partial D_{i,j}} - \fint_{\partial D_{i,j}} \Big] \nabla \mathcal{I}_h u \cdot \vec{n}_{i,j} ds \right|, \tag{4.15}$$

where $\vec{n}_{i,j}$ is a unit vector normal to $\partial D_{i,j}$ and directed toward D_j (2.17). Since the integration rule $\int_{\partial D_{i,j}}$ integrates the polynomials of $k-1$ exactly, we have

$$\begin{aligned} \left| \Big[\int_{\partial D_{i,j}} - \fint_{\partial D_{i,j}} \Big] \nabla \mathcal{I}_h u \cdot \vec{n}_{i,j} ds \right| &= \left| \Big[\int_{\partial D_{i,j}} - \fint_{\partial D_{i,j}} \Big] \nabla \big(\mathcal{I}_h u - T_i^k \mathcal{I}_h u \big) \cdot \vec{n}_{i,j} ds \right| \\ &\le Ch^{k+d-1} |u|_{W^{k+1,\infty}(\Omega)}, \end{aligned}$$

where the last inequality comes from (4.13), (4.14), and a fact $|\partial D_{i,j}| \le Ch^{d-1}$. Using this estimate and (2.9) in (4.15), we have

$$\begin{aligned} |A_h^*(\mathcal{I}_h u, w_h) - \tilde{A}_h^*(\mathcal{I}_h u, w_h)| &\le Ch^{k+d-1} |u|_{W^{k+1,\infty}(\Omega)} \sum_{i \in N_h} \left(\sum_{j \in \check{S}_i} (w_j - w_i)^2 \right)^{1/2} \\ &\le Ch^{k+d-1} |u|_{W^{k+1,\infty}(\Omega)} \left(\sum_{i \in N_h} \big(\sum_{j \in \check{S}_i} (w_j - w_i)^2 \big) \right)^{1/2} \left(\sum_{i \in N_h} 1 \right)^{1/2} \\ &\le Ch^{k+d-1} h^{\frac{2-d}{2}} |u|_{W^{k+1,\infty}(\Omega)} |w_h|_{H^1(\Omega)} h^{-\frac{d}{2}} = Ch^k |u|_{W^{k+1,\infty}(\Omega)} |w_h|_{H^1(\Omega)}. \end{aligned} \tag{4.16}$$

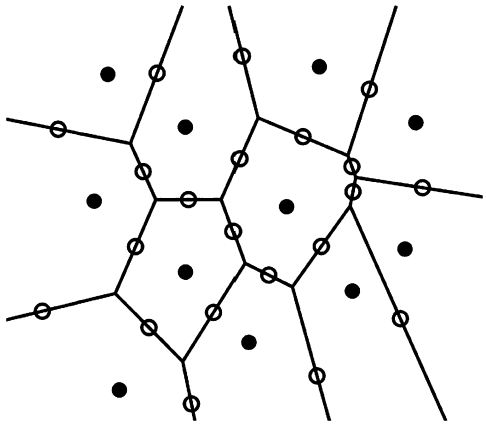

Fig. 2. An illustration on numerical integration for $k = 1, 2$: one-point Gaussian rule ($\circ$) on each side of the sub-region is sufficient to produce the optimal convergence rate.

Next, it can be shown that

$$L_h^*(w_h) - \tilde{L}_h^*(w_h) = \sum_{i\in N_h} w_i \Big[\int\!\!\!\!\!\!- \Big]_{D_i} f(x)dx + \sum_{i\in N_h'} w_i \Big[\int\!\!\!\!\!\!- \Big]_{D_i\cap\Gamma} g(s)ds. \tag{4.17}$$

Similarly,

$$\left| \Big[\int\!\!\!\!\!\!- \Big]_{D_i} f(x)dx \right| = \left| \Big[\int\!\!\!\!\!\!- \Big]_{D_i} \big(f(x) - T_i^{k-1} f(x)\big)dx \right| \le Ch^{k+d} |f|_{W^{k,\infty}(\Omega)}$$

and

$$\begin{aligned} \left| \Big[\int\!\!\!\!\!\!- \Big]_{D_i\cap\Gamma} g(s)ds \right| &= \left| \Big[\int\!\!\!\!\!\!- \Big]_{D_i\cap\Gamma} \big(g(s) - T_i^{k-1} g(s)\big)ds \right| \\ &\le Ch^{k+d-1} |g|_{W^{k,\infty}(\Gamma)} \le Ch^{k+d-1} |u|_{W^{k+1,\infty}(\Omega)}. \end{aligned}$$

Using these two estimates, (2.7), and (2.8) in (4.17), we have

$$\begin{aligned} |L_h^*(w_h) - \tilde{L}_h^*(w_h)| &\le Ch^{k+d} |f|_{W^{k,\infty}(\Omega)} \Big(\sum_{i\in N_h} w_i^2 \Big)^{1/2} \Big(\sum_{i\in N_h} 1 \Big)^{1/2} \\ &\quad + Ch^{k+d-1} |u|_{W^{k+1,\infty}(\Omega)} \Big(\sum_{i\in N_h'} w_i^2 \Big)^{1/2} \Big(\sum_{i\in N_h} 1 \Big)^{1/2} \\ &\le Ch^{k+d} |f|_{W^{k,\infty}(\Omega)} h^{-\frac{d}{2}} \|w_h\|_{L^2(\Omega)} h^{-\frac{d}{2}} + Ch^{k+d-1} |u|_{W^{k+1,\infty}(\Omega)} h^{-\frac{d-1}{2}} \|w_h\|_{L^2(\Gamma)} h^{-\frac{d-1}{2}}. \end{aligned} \tag{4.18}$$

Remember that we impose the condition $w_h(z_0) = 0, \forall\ w_h \in U_h$ to ensure a unique solution to the pure Neumann problem in Remark 2.4. Then according to the Poincaré inequality and the trace inequality, we have

$$\|w_h\|_{L^2(\Omega)} \le C|w_h|_{H^1(\Omega)} \quad \text{and} \quad \|w_h\|_{L^2(\Gamma)} \le \|w_h\|_{H^1(\Gamma)} \le |w_h|_{H^1(\Gamma)}.$$

Based on this, (4.18), (4.16), (4.12), and (2.19), we get

$$|u - \tilde{u}_h|_{H^1(\Omega)} \le |u - \mathcal{I}_h u|_{H^1(\Omega)} + |\tilde{u}_h - \mathcal{I}_h u|_{H^1(\Omega)} \le Ch^k |u|_{W^{k+1,\infty}(\Omega)} + Ch^k |f|_{W^{k,\infty}(\Omega)},$$

which proves the estimate (4.11). □

Remark 4.1. The optimal convergence rate $O(h^k)$ in the energy norm is derived in Theorem 4.1 for the proposed MFVM with numerical integration. We will also test the convergence rate (4.11) numerically in the next section. The numerical integration rules in Theorem 4.1 are easy to implement. For example, we consider the two-dimensional problem with $k = 1, 2$. In this case, the one-point Gaussian rule on $\partial D_{i,j}$ (exact for linear polynomials on $\partial D_{i,j}$) is sufficient to achieve the optimal error estimate. See Fig. 2. The complexity in the numerical integration is almost the same as the nodal integration [9,16], and the computing cost is much cheaper than other integration rules in the MM.

5. Direct imposition of the EBC

In this section, we emphasize on the treatment of the EBC in the proposed MFVM. We will prove that the EBC can be imposed directly on the boundary particles. It will also be demonstrated that the Kronecker property of the shape functions ϕ_i may not be necessary for the meshfree particle methods. We consider the model problem (2.1) with an essential boundary condition

$$\begin{aligned} -\triangle u &= f, \quad \text{in } \Omega \\ u &= u_0, \quad \text{on } \Gamma. \end{aligned} \tag{5.1}$$

For convenience, we divide N_h into two parts: $N_h' = \{i \in N_h : x_i \in \Gamma\}$ and $N_h'' = N_h \backslash N_h'$. Namely, the particles $x_i \in N_h'$ and $x_i \in N_h''$ are located on the boundary Γ and inside Ω, respectively. Denote

$$U_h'' = \text{span}\{\phi_j : j \in N_h''\} \text{ and } U_h' = \text{span}\{\phi_j : j \in N_h'\}.$$

For any $v \in H^2(\overline{\Omega})$, we define

$$\mathcal{I}_h'' v := \sum_{i \in N_h''} v(x_i)\phi_i \text{ and } \mathcal{I}_h' v := \sum_{i \in N_h'} v(x_i)\phi_i,$$

which are the interpolants of v in U_h'' and U_h', respectively. For any $i \in N_h''$, multiplying two sides of (5.1) by $\mathbf{1}_{D_i}$ and using the integration by parts, we obtain

$$-\int_{\partial D_i} \nabla u \cdot \vec{n}_i ds = \int_{D_i} f(x)dx, \ \forall\ i \in N_h''. \tag{5.2}$$

For any $v_h'' = \sum_{i \in N_h''} c_i \phi_i \in U_h''$, denote

$$F_h^*(v_h'') := \sum_{i \in N_h''} c_i \left(\int_{D_i} f(x)dx \right).$$

Then (5.2) is equivalent to

$$A_h^*(u, v_h'') = F_h^*(v_h''), \ \forall\ v_h'' = \sum_{i \in N_h''} c_i \phi_i \in U_h'', \tag{5.3}$$

where A_h^* was defined in (2.15).

To discretize (5.3), we consider a discrete variational formulation as follows:

$$\text{Find } \mathcal{I}_h' u_0 + u_h'' \text{ with } u_h'' \in U_h'', \text{ such that } A_h^*(\mathcal{I}_h' u_0 + u_h'', v_h'') = F_h^*(v_h''), \ \forall\ v_h'' \in U_h''. \tag{5.4}$$

Obviously, the formulation (5.4) is the same as

$$\text{Find } u_h'' \in U_h'', \text{ such that } A_h^*(u_h'', v_h'') = F_h^*(v_h'') - A_h^*(\mathcal{I}_h' u_0, v_h''), \ \forall\ v_h'' \in U_h''. \tag{5.5}$$

The inf-sup condition of the bilinear form $A_h^*(\cdot,\cdot)$ on U_h'' can be established using the same way in Section 3. This ensures the unique solvability of (5.5) or (5.4). According to (5.3) and (5.4), we have

$$A_h^*(u - \mathcal{I}_h' u_0 - u_h'', v_h'') = 0, \ \forall\ v_h'' \in U_h''. \tag{5.6}$$

Then, using the equation (5.6) and the similar argument as in Theorem 2.1, we have

$$|u - \mathcal{I}_h' u_0 - u_h''|_{H^1(\Omega)} \le C \inf_{w_h \in U_h''} (|u - \mathcal{I}_h' u_0 - w_h''|_{H^1(\Omega)} + h|u - \mathcal{I}_h' u_0 - w_h''|_{H^2(\Omega)}). \tag{5.7}$$

Therefore, letting $w_h'' = \mathcal{I}_h'' u$ in (5.7) and noting the EBC $u = u_0$ on Γ, we have

$$\begin{aligned} |u - \mathcal{I}_h' u_0 - u_h''|_{H^1(\Omega)} &\le C|u - \mathcal{I}_h' u_0 - \mathcal{I}_h'' u|_{H^1(\Omega)} + h|u - \mathcal{I}_h' u_0 - \mathcal{I}_h'' u|_{H^2(\Omega)}) \\ &= C(|u - \mathcal{I}_h u|_{H^1(\Omega)} + h|u - \mathcal{I}_h u|_{H^2(\Omega)}) \le Ch^k \|u\|_{W^{k+1,\infty}(\Omega)}, \end{aligned} \tag{5.8}$$

where the last equality is due to the interpolation error estimate (2.10).

Remark 5.1. Clearly, the estimate (5.8) shows that u is approximated by $\mathcal{I}'_h u_0 + u''_h$ with the optimal convergence order. $\mathcal{I}'_h u_0 + u''_h$ is solved from the discrete variational problem (5.4). It is important to note that $\mathcal{I}'_h u_0$ is the interpolant of u based on the particles on the boundary Γ, which is given according to the EBC $u = u_0$ on Γ. This implies that the EBC is imposed directly on the boundary particles in the MFVM, even though the trial shape functions ϕ_i's do not satisfy the Kronecker property.

In many MMs, there exist the test functions ψ_i, associated with the interior particles $x_i, i \in N''_h$, whose supports may intersect with the boundary. Multiplying two sides of (5.1) by such ψ_i and making the integration by part generate that

$$\int_{\omega_i} \nabla u \cdot \nabla \psi_i \, dx - \int_{\omega_i \cap \Gamma} \frac{\partial u}{\partial n} \psi_i \, ds = \int_{\omega_i} f \, \psi_i \, dx, \quad \forall \ p \in \mathcal{P}_k. \tag{5.9}$$

Comparing (5.9) with (5.2), we note that there is a nonconforming term $\int_{\omega_i \cap \Gamma} \frac{\partial u}{\partial n} \psi_i ds$ in (5.9), where $\frac{\partial u}{\partial n}$ is unknown on Γ. This creates the difficulties in directly imposing EBC in the MMs. Thus, various special treatments were proposed to manage the conforming errors, such as penalty techniques. In the proposed MFVM, the supports of test functions $\psi_i = \mathbf{1}_{D_i}, i \in N''_h$ do not intersect with the boundary Γ, and the EBC can be enforced directly, as demonstrated in (5.4) and (5.8).

6. Numerical tests

The numerical results are reported to verify the theoretical results in Sections 4 and 5. We only consider the EBC (5.1) to demonstrate that the proposed MFVM can address the numerical integration and the imposition of the EBC simultaneously.

For comparison, we also present the numerical results of the conventional MM (2.11) where both the trial and the test spaces are U_h. We use the numerical integration rules for the MFVM that satisfy the conditions in Theorem 4.1. Namely, $f_{\partial D_{i,j}}, j \in \tilde{S}_i$ and f_{D_i} are exact for polynomials of degree $k-1$ on $\partial D_{i,j}$ and D_i, respectively; and $f_{D_i \cap \Gamma}$ is exact for polynomials of degree $k-1$ on $D_i \cap \Gamma$. Therefore, we use one-point Gaussian rules on $f_{\partial D_{i,j}}$ and f_{D_i}, respectively, since we consider the cases $k = 1, 2$, see Remark 4.1. We use a background integration scheme for the conventional MM. Specifically, we use 5-point and 5×5 Gaussian rules on each background portion for one-dimensional and two-dimensional problems, respectively.

The EBC will be imposed directly on the boundary nodes for both the MFVM and the MM. The optimal convergence rate of the MFVM with the direct imposition of EBC was proven in Section 5. There are various approaches to enforce the EBC in the conventional MM, such as the Lagrange multiplier, the penalty methods, and coupling with the FEM. We do not present these methods since we would like to show that it is feasible for the MFVM to impose the EBC directly without special treatments.

We will also test the inf-sup constant λ_{IS} defined below (3.7) in Section 3 and compare the relative errors of the MFVM and the MM as follows:

$$EE := \frac{|u - u_N|_{H^1(\Omega)}}{|u|_{H^1(\Omega)}},$$

where u_N is an MFVM or MM solution.

We first test a one-dimensional problem. Let $\Omega = (0, 1)$ and $\Gamma = \{0, 1\}$, then the model problem with the EBC is

$$-u'' = f(x) \quad \text{in } \Omega, \ \text{ and } \ u(0) = u_0(0), \ \ u(1) = u_0(1). \tag{6.1}$$

We assume that $u(x) = e^{5x}$ is the exact solution, and the $f(x)$ and $u_0(x)$ are calculated through equation (6.1) using u. Let $\{x_i : i = 1, \cdots, N\}$ with $x_1 = 0, x_N = 1$ be the particles in $\bar{\Omega}$, and each x_i is associated with a weight function $w_i(x) := \tilde{w}(\frac{x - x_i}{r_i})$, where $\tilde{w}$ is a cubic spline reference function as follows:

$$\tilde{w}(x) = \begin{cases} \frac{2}{3} - 4x^2 + 4|x|^3, & |x| \le \frac{1}{2} \\ \frac{4}{3} - 4|x| + 4x^2 - \frac{4}{3}|x|^3, & \frac{1}{2} < |x| \le 1 \\ 0, & |x| > 1 \end{cases}, \tag{6.2}$$

and r_i controls the support of w_i. The trial function space $U_h = \{\phi_i : i = 1, 2, \cdots, N\}$ is constructed according to x_i and w_i using the standard MLS or RKP procedures. These shape functions satisfy the polynomial reproducing property as follows:

$$\sum_{i=1}^{N} x_i^l \phi_i(x) = x^l, \ \ l = 0, 1, \cdots, k.$$

In the numerical experiments we only consider the cases $k = 1, 2$ that are most frequently applied in practice. The associated Voronoi diagram consists of $[\bar{x}_{i-1}, \bar{x}_i]$, $i = 1, 2, \cdots, N$, where $\bar{x}_i = \frac{1}{2}(x_i + x_{i+1})$, $i = 1, 2, \cdots N-1$, and $\bar{x}_0 = x_1, \bar{x}_N = x_N$. Therefore, the test space V_h is given by

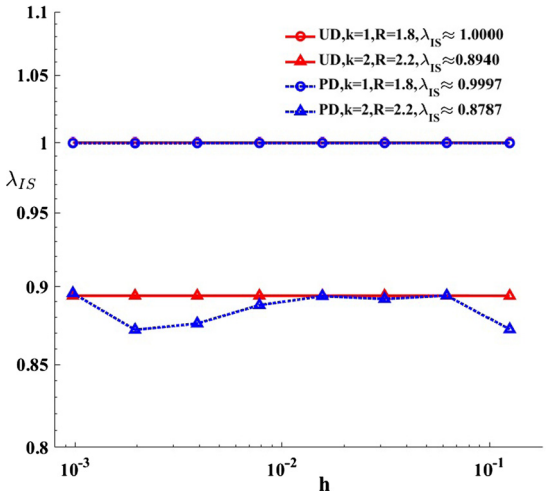

Fig. 3. The inf-sup constant λ_{IS} with respect to $h = \frac{1}{N-1}$ with $N = 2^{i+2} + 1$, $i = 1, 2, \cdots, 8$ for one dimensional uniformly distributed (UD) and perturbed (PD) particles.

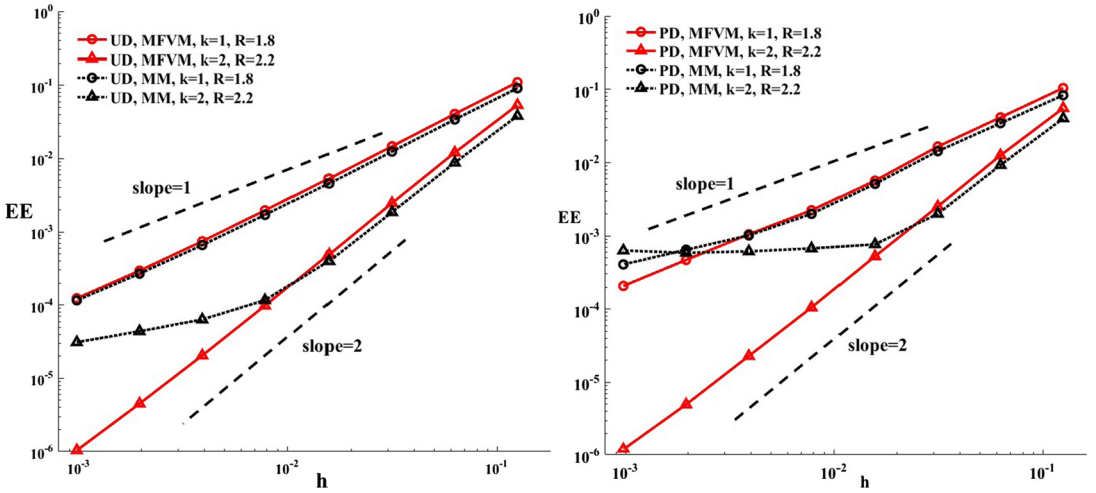

Fig. 4. The relative errors EE with respect to $h = \frac{1}{N-1}$ with $N = 2^{i+2} + 1$, $i = 1, 2, \cdots, 8$ for the one-dimensional uniformly distributed (UD) (left) and perturbed (PD) (right) particles.

$$V_h = \text{span}\{\mathbf{1}_{[\bar{x}_{i-1}, \bar{x}_i]} : i = 1, 2, \cdots, N\}.$$

Two particle distributions are considered as follows:

- uniform distribution (UD): $x_i = \frac{i-1}{N-1}$ and $r_i = Rh$, $i = 1, 2, \cdots, N$, where $h := \frac{1}{N-1}$ and R is a constant independent of h and i;
- perturbed distribution (PD): $x_i = \frac{i-1}{N-1} + 0.1h\epsilon_i$, $i = 2, \cdots, N-1$, $x_1 = 0$, $x_N = 1$, and $r_i = Rh$, where ϵ_i is a random number produced from an uniform distribution on $[-0.5, 0.5]$.

The inf-sup constant λ_{IS} and the relative errors (EE) of the MFVM and the MM for $k = 1, 2$ are presented in Fig. 3 and Fig. 4. We take $R = 1.8$ for $k = 1$ and $R = 2.2$ for $k = 2$ in the tests. We also examined different values of R and attained similar results. It can be seen in Fig. 3 that for both the uniform and perturbed particle distributions, the inf-sup constants have lower bounds as h becomes small. This verifies the inf-sup conditions (2.18) and (4.6). The approximation errors (EE) in the energy norm decrease with the optimal rate $O(h^k), k = 1, 2$, as predicted in Theorem 4.1. The direct imposition of the EBC causes serious errors in the MM, especially for $k = 2$; while it works very well for the MFVM, as analyzed in Section 5. See Fig. 4.

We next present a two-dimensional numerical experiment. Let $\Omega = (0, 1) \times (0, 1)$ and $\Gamma = \partial\Omega$. Assume $u(x) = e^{2\xi+\eta}$ is the exact solution, where $x = (\xi, \eta)$ is the Cartesian coordinates in $\mathbb{R}^2$. Then the model problem (5.1) with the EBC is

$$-\triangle u = -5e^{2\xi+\eta} \quad \text{in } \Omega$$

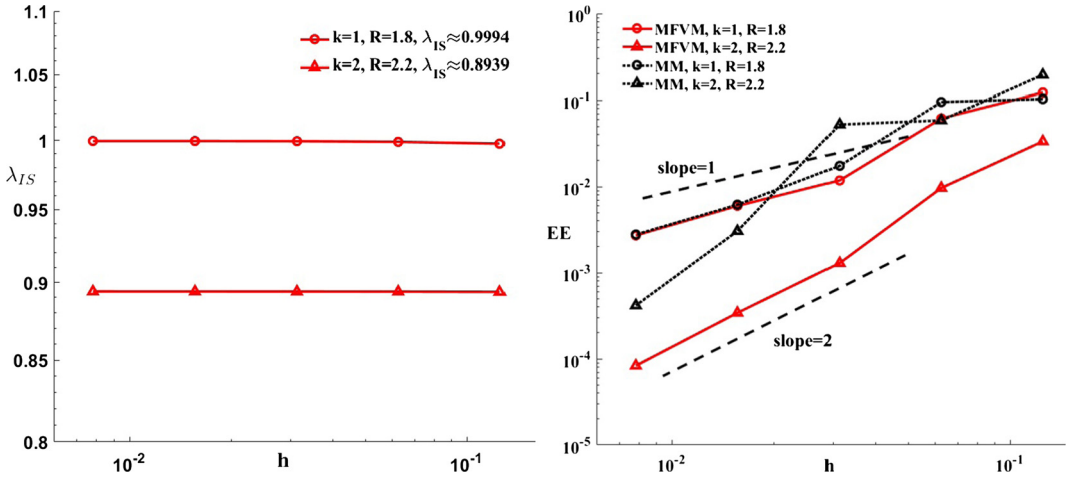

Fig. 5. The inf-sup constant λ_{IS} (left) and the relative errors EE (right) with respect to $h = \frac{1}{N-1}$ with $N = 2^{i+2} + 1$, $i = 1, 2, \cdots, 5$ for two-dimensional uniformly distributed particles.

$$u(x) = e^{2\xi+\eta} \quad \text{on } \Gamma.$$

We consider the particles $\{x_{ij} = (\xi_i, \eta_j), i, j = 1, 2, \cdots, N\}$ on Ω, where $\xi_i = \frac{i-1}{N-1}$, $\eta_j = \frac{j-1}{N-1}$, and the weight functions $w_{ij} = w_i(\xi) w_j(\eta)$. The trial function space $U_h = \{\phi_{ij} : i, j = 1, 2, \cdots, N\}$ is constructed according to x_{ij} and w_{ij} using the standard MLS or RKP procedures. These shape functions satisfy the polynomial reproducing property as follows:

$$\sum_{i,j=1}^{N} x_{ij}^{\beta} \phi_{ij}(x) = x^{\beta}, \ \forall\, x \in \Omega \text{ and } |\beta| = 0, 1, \cdots, k. \tag{6.3}$$

The associated Voronoi diagram consists of $[\bar{\xi}_{i-1}, \bar{\xi}_i] \times [\bar{\eta}_{i-1}, \bar{\eta}_i]$, $i, j = 1, 2, \cdots, N$, where $\bar{\xi}_i = \frac{1}{2}(\xi_i + \xi_{i+1})$, $i = 1, 2, \cdots N-1$, and $\bar{\xi}_0 = \xi_1, \bar{\xi}_N = \xi_N$, and $\bar{\eta}_j = \frac{1}{2}(\eta_j + \xi_{j+1})$, $j = 1, 2, \cdots N-1$, and $\bar{\eta}_0 = \eta_1, \bar{\eta}_N = \eta_N$ Therefore, the test space V_h is given by

$$V_h = \text{span}\{\mathbf{1}_{[\bar{\xi}_{i-1}, \bar{\xi}_i] \times [\bar{\eta}_{i-1}, \bar{\eta}_i]} : i = 1, 2, \cdots, N\}.$$

The one-point Gaussian rule is used in the MFVM for the cases $k = 1, 2$; while 5×5-Gaussian rules are employed on each background portion $[\xi_{i-1}, \xi_i] \times [\eta_{j-1}, \eta_j]$ for the MM. The inf-sup constants λ_{IS} and the EEs of the MFVM and the MM for $k = 1, 2$ are presented in Fig. 5. Similar to the one-dimensional results, the inf-sup constants have the lower bounds as h decreases, and the inf-sup conditions (2.18) and (4.6) are verified. The optimal approximation errors (EE) $O(h^k), k = 1, 2$, are shown in Fig. 5 (right) to verify the result in Theorem 4.1. The direct imposition of the EBC is applied successfully in the MFVM, as analyzed in Section 5.

7. Conclusion

The MFVM proposed in this paper simultaneously addressed the main difficulties in the MM, the numerical integration and imposition of the EBC. The standard Gaussian rules were proven to produce the optimal approximation errors $O(h^k)$, and the EBC can be imposed directly on the boundary nodes. The inf-sup conditions for the MFVM were proven in a one-dimensional problem and verified numerically using a generalized eigenvalue problem for higher dimensions. For the non-smooth problems, such as interface problems, the trial functions ϕ_i need to be constructed by including various non-polynomial functions that mimic the non-smooth features of exact solutions. Detailed investigation in this regard will be conducted in a forthcoming study.

References

[1] S.N. Atluri, S. Shen, The Meshless Local Petrov Galerkin Method, Tech. Sci. Press, 2002.
[2] S.N. Atluri, S. Shen, The meshless local Petrov-Galerkin (MLPG) method: a simple & less-costly alternative to the finite element and boundary element methods, Comput. Model. Eng. Sci. 3 (2002) 11–51.
[3] S.N. Atluri, Z.D. Han, A.M. Rajendran, A new implementation of the meshless finite volume method, through the MLPG "mixed" approach, Comput. Model. Eng. Sci. 6 (2004) 491–513.
[4] I. Babuška, U. Banerjee, J. Osborn, Survey of meshless and generalized finite element methods: a unified approach, Acta Numer. 12 (2003) 1–125.
[5] I. Babuška, U. Banerjee, J. Osborn, Q. Li, Quadrature for meshless methods, Int. J. Numer. Methods Eng. 76 (2008) 1434–1470.
[6] I. Babuška, U. Banerjee, J. Osborn, Q. Zhang, Effect of numerical integration on meshless methods, Comput. Methods Appl. Mech. Eng. 198 (2009) 2886–2897.

[7] T. Barth, M. Ohlberger, Finite volume methods: foundation and analysis, in: Encyclopedia of Computational Mechanics, vol. 1, Wiley, Chichester, England, 2004, Chapter 15.
[8] L. Beirão Da Veiga, F. Brezzi, A. Cangiani, G. Manzini, L.D. Marini, A. Russo, Basic principles of virtual element methods, Math. Models Methods Appl. Sci. 23 (2013) 199–214.
[9] S. Beissel, T. Belytschko, Nodal integration of the element-free Galerkin method, Comput. Methods Appl. Mech. Eng. 139 (1996) 49–74.
[10] T. Belytschko, Y. Krongauz, D. Organ, M. Fleming, P. Krysl, Meshless methods: an overview and recent developments, Comput. Methods Appl. Mech. Eng. 139 (1996) 3–47.
[11] T. Belytschko, Y.Y. Lu, L. Gu, Element-free Galerkin methods, Int. J. Numer. Methods Eng. 37 (1994) 229–256.
[12] Z. Cai, On the finite volume element method, Numer. Math. 58 (1991) 713–735.
[13] A. Carpinteri, G. Ferro, G. Ventura, The partition of unity quadrature in meshless methods, Int. J. Numer. Methods Eng. 54 (2002) 987–1006.
[14] J.-S. Chen, M. Hillman, M. Rüter, An arbitrary order variationally consistent integration for Galerkin meshfree methods, Int. J. Numer. Methods Eng. 95 (2013) 387–418.
[15] J.-S. Chen, M.ASCE, M. Hillman, S. Chi, Meshfree methods: progress made after 20 years, J. Eng. Mech 143 (2017) 04017001.
[16] J.-S. Chen, C.-T. Wu, S. Yoon, Y. You, A stabilized conformal nodal integration for a Galerkin mesh-free method, Int. J. Numer. Methods Eng. 50 (2001) 435–466.
[17] Z. Chen, Y. Xu, Y. Zhang, A construction of higher-order finite volume methods, Math. Comput. 84 (292) (2015) 599–628.
[18] P.G. Ciarlet, The Finite Element Method for Elliptic Problems, North-Holland, Amsterdam, 1978.
[19] L. Cueto-Felgueroso, I. Colominas, J. Fe, F. Navarrina, M. Casteleiro, High-order finite volume schemes on unstructured grids using moving least-squares reconstruction. Application to shallow water dynamics, Int. J. Numer. Methods Eng. 65 (2006) 295–331.
[20] S. De, K.J. Bathe, The method of finite squares with improved numerical integration, Comput. Struct. 79 (2001) 2183–2196.
[21] J. Dolbow, T. Belytschko, Numerical integration of the Galerkin weak form in meshfree methods, Comput. Mech. 23 (1999) 219–230.
[22] Q. Duan, T. Belytschko, Gradient and dilatational stabilizations for stress-point integration in the element-free Galerkin method, Int. J. Numer. Methods Eng. 77 (2009) 776–798.
[23] Q. Duan, X. Li, H. Zhang, T. Belytschko, Second-order accurate derivatives and integration schemes for meshfree methods, Int. J. Numer. Methods Eng. 92 (2012) 399–424.
[24] M.S. Ebeida, S.A. Mitchell, Uniform random Voronoi meshes, in: Proceedings of the 20th International Meshing Roundtable, IMR 2011, 2011, pp. 273–290.
[25] S. Fernandez-Mendez, A. Huerta, Imposing essential boundary conditions in mesh-free methods, Comput. Methods Appl. Mech. Eng. 193 (2004) 1257–1275.
[26] G. Fougeron, D. Aubry, Imposition of boundary conditions for elliptic equations in the context of non boundary fitted meshless methods, Comput. Methods Appl. Mech. Eng. 343 (2019) 506–529.
[27] T.-P. Fries, T. Belytschko, Convergence and stabilization of stress-point integration in mesh-free and particle methods, Int. J. Numer. Methods Eng. 74 (2008) 1067–1087.
[28] M. Griebel, M.A. Schweitzer, A particle-partition of unity method. II. Efficient cover construction and reliable integration, SIAM J. Sci. Comput. 23 (2002) 1655–1682.
[29] M. Griebel, M.A. Schweitzer, A particle-partition of unity method. V. Boundary conditions, in: Geometric Analysis and Nonlinear Partial Differential Equations, Springer, Berlin, 2003, pp. 519–542.
[30] W. Han, X. Meng, Error analysis of the reproducing kernel particle method, Comput. Methods Appl. Mech. Eng. 190 (2001) 6157–6181.
[31] A. Huerta, S. Fernandez-Mendez, Enrichment and coupling of the finite element and meshless methods, Int. J. Numer. Methods Eng. 48 (2000) 1615–1636.
[32] G.R. Joldes, H. Chowdhury, A. Wittek, K. Miller, A new method for essential boundary conditions imposition in explicit meshless methods, Eng. Anal. Bound. Elem. 80 (2017) 94–104.
[33] M. Juntunen, R. Stenberg, Nitsche's method for general boundary conditions, Math. Comput. 78 (2009) 1353–1374.
[34] Y. Krongauz, T. Belytschko, Enforcement of essential boundary conditions in meshless approximations using finite elements, Comput. Methods Appl. Mech. Eng. 131 (1996) 133–145.
[35] R. Li, Z. Chen, W. Wu, The Generalized Difference Methods for Partial Differential Equations, Marcel Dikker, New York, 2000.
[36] S. Li, W.K. Liu, Meshfree and particle methods and their application, Appl. Mech. Rev. 55 (2002) 1–34.
[37] Y. Lin, M. Yang, Q. Zou, L^2 error estimates for a class of any order finite volume schemes over quadrilateral meshes, SIAM J. Numer. Anal. 53 (2015) 2030–2050.
[38] Y. Liu, T. Belytschko, A new support integration scheme for the weakform in mesh-free methods, Int. J. Numer. Methods Eng. 82 (2010) 699–715.
[39] W.K. Liu, S. Jun, Y.F. Zhang, Reproducing kernel particle methods, Int. J. Numer. Methods Fluids 20 (1995) 1081–1106.
[40] J.M. Melenk, On approximation in meshless methods, in: J. Blowey, A. Craig (Eds.), Frontiers in Numerical Analysis, Durham 2004, Springer Verlag, 2005.
[41] J. Nitsche, Über ein variationsprinzip zur lösung von Dirichlet-problemen bei verwendung von teilräumen, die keinen randbedingungen unterworfen sind, Abh. Math. Semin. Univ. Hamb. 36 (1970–1971) 9–15.
[42] N. Sukumar, B. Moran, T. Belytschko, The natural element method in solid mechanics, Int. J. Numer. Methods Eng. 43 (1998) 839–887.
[43] L. Sun, G. Yang, Q. Zhang, Numerical integration with constraints for meshless local Petrov-Galerkin methods, Comput. Model. Eng. Sci. 95 (2013) 235–258.
[44] Q. Zhang, Theoretical analysis of numerical integration in the Galerkin meshless methods, BIT Numer. Math. 51 (2011) 459–480.
[45] Q. Zhang, Quadrature for meshless Nitsche's methods, Numer. Methods Partial Differ. Equ. 30 (2014) 265–288.
[46] Q. Zhang, U. Banerjee, Numerical integration in Galerkin meshless methods, applied to elliptic Neumann problem with non-constant coefficients, Adv. Comput. Math. 37 (2012) 453–492.
[47] Z. Zhang, Q. Zou, Vertex-centered finite volume schemes of any order over quadrilateral meshes for elliptic boundary value problems, Numer. Math. 130 (2015) 363–393.
[48] H. Zheng, W. Li, X. Du, Exact imposition of essential boundary condition and material interface continuity in Galerkin-based meshless methods, Int. J. Numer. Methods Eng. 110 (2017) 637–660.
[49] T. Zhu, S.N. Atluri, A modified collocation method and penalty formulation for enforcing the essential boundary conditions in the element free Galerkin method, Comput. Mech. 21 (1998) 211–222.